External Feedback Effect in Terahertz Resonant Tunneling Diode Oscillators

Luong Duy Manh ⬛ , *Member, IEEE*, Sebastian Diebold, *Member, IEEE*, Kousuke Nishio, Yousuke Nishida, Jaeyoung Kim, Toshikazu Mukai, Masayuki Fujita ⬛ , *Member, IEEE*, and Tadao Nagatsuma ⬛ , *Fellow, IEEE*

Abstract—The external feedback effect of a resonant tunneling diode oscillator in terahertz (THz) proximity wireless transmission is modeled and analyzed. The model is based on the circuit modeling of the resonant tunneling diode and the passive structures. We investigate important system parameters such as the reflectivities at the transmitter and the receiver and the power coupling. It is found that the frequency change, the frequency change rate, and the direct-current change are mainly dependent on the reflectivity at the receiver. The received power change is mainly caused by the reflectivity at the transmitter. The simulations agree well with the experimental results. In addition, we demonstrate the high accuracy of our models by clarifying origins of the bit-error-rate change with distance. This demonstrates that the proposed model can be used for the design of a stable THz proximity wireless communication system. The model is also considered to be potentially applicable in other promising THz applications including sensing and radar.

Index Terms—External feedback, radar, resonant tunneling diode (RTD), sensing, terahertz (THz), wireless communication.

I. Introduction

TERAHERTZ (THz) waves are currently being extensively studied because of promising applications including high-capacity wireless communication, high-resolution imaging, and high-sensitivity sensing [1]–[10]. Resonant tunneling diodes (RTDs) are becoming one of the most promising THz sources, thanks to their room temperature operation, compact size, cost effectiveness, and high-frequency oscillation [11]–[16]. With a reported oscillation frequency of 1.92 THz at room temperature

[17], RTDs can be utilized for a wide variety of important applications in wireless communication [18]–[23], imaging [24], as well as in sensing [25]. In these RTD-based applications, the transmission distance between the RTD transmitter (Tx) and receiver (Rx) is limited to a short distance due to the low output power of the RTD Tx and strong attenuation of the THz wave in air [26]. This leads to a complex and important effect called external feedback, which is caused by the standing wave on the THz transmission link [27], [28]. This standing wave occurs, when part of the THz signal is reflected back to the RTD Tx, when it reaches the Rx. As a result, not only the oscillation frequency but the received power and direct current (dc) of the RTD oscillator can easily change with the distance between the Tx and the Rx. These changes contribute both negatively and positively. In wireless communication, any change in the frequency or power is not desired, particularly when using frequency- or phase-based modulation schemes such as quadrature amplitude modulation (QAM) or quadrature phase-shift keying (QPSK). On the other hand, in sensing and radar applications, frequency or dc current changes may play important roles in targeting objects and in the sensing properties of the system, such as the reflectivities at the Tx and the Rx or the power coupling efficiency and power loss factors. Consequently, understanding and modeling the external feedback effect will contribute significantly to the design of various promising THz applications. To the best of our knowledge, Asada and Suzuki [27] were the first to report this RTD oscillator effect. Their analysis demonstrates that the frequency change is directly proportional to the load reflectivity and inversely proportional to the Q-factor of the RTD oscillator. Moreover, they also showed that the frequency changes periodically as a function of the distance between the Tx and the Rx, and of the load reflectivity phase by a sinusoidal function. However, their theory is not supported by experimental data. In addition, realistic models consisting of the most of essential components of the Tx and Rx were not considered practically. However, in this study, we construct a complete model to effectively describe the external feedback effect in the 300-GHz band by considering various critical factors of the system. Our model is then validated by measurements. The rest of this paper is organized as follows. The constructed model and various investigations on the external feedback effect are presented in Section II. The simulated results are then validated by measurements in Section III. After validating with measurements, the contribution of the model to wireless communication is demonstrated in Section IV. Section V summarizes this paper.

L. D. Manh was with the Graduate School of Engineering Science, Osaka University, Osaka 560-8531, Japan. He is now with the Faculty of Radio-Electronic Engineering, Le Quy Don Technical University, Hanoi 100000, Vietnam (e-mail: duymanhcs2@mta.edu.vn).

S. Diebold was with the Graduate School of Engineering Science, Osaka University, Osaka 560-8531, Japan. He is now with pSemi (a Murata Company), San Diego, CA 92121 USA (e-mail: diebold@laser.ee.es.osaka-u.ac.jp).

K. Nishio, Y. Nishida, M. Fujita, and T. Nagatsuma are with the , Graduate School of Engineering ScienceOsaka University, Osaka 560-8531, Japan (e-mail: kousukenishio118@s.ee.es.osaka-u.ac.jp; yousukenishida127@s.ee.es.osaka-u.ac.jp; fujita@ee.es.osaka-u.ac.jp; nagatuma@ee.es.osaka-u.ac.jp).

J. Kim and T. Mukai are with the , Fundamental Research and Development Division, ROHM Co., Ltd., Kyoto 615-8585, Japan (e-mail: jaeyoung.kim@dsn.rohm.co.jp; toshikazu.mukai@dsn.rohm.co.jp).
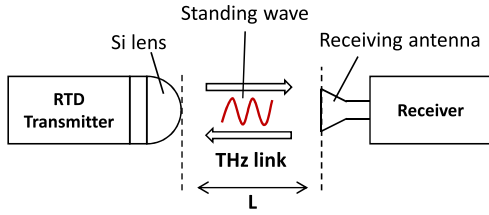
Fig. 1. Illustration of the external feedback effect on RTD-based systems. Here, L is the spacing between the Tx and the Rx.
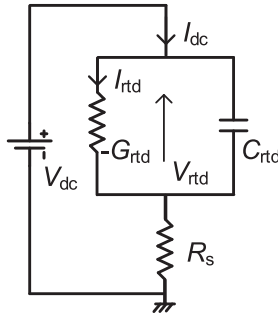

Fig. 2. Equivalent circuit of an intrinsic RTD.

II. Model Construction

In this section, the external feedback effect is modeled, based on the circuit simulation method. Because this effect relates to all the components of the RTD-based system such as the Tx, Rx, and THz link, every individual component must be modeled. Fig. 1 shows the simplified illustration of the external feedback in the RTD-based system. External feedback is caused by the standing wave of the THz link, which occurs due to the interference between the transmitted and reflected THz signals. The following subsections present the modeling procedure for each component of the system.

A. RTD Oscillator Modeling

The RTD oscillator consists of an RTD, a resonator line, and an antenna. In contrast to the RTD model in [28], which has a polynomial-based current and a voltage-independent capacitance, the present RTD model employs a more complex current model and a voltage-dependent capacitance. This capacitance model includes both static and dynamic capacitances, while the complex current contains three current components: coherent tunneling current, excess current, and perimeter-dependent sidewall current. A detailed description of this RTD model is given in [30]. The equivalent circuit of the intrinsic RTD is illustrated in Fig. 2. As can be seen that the RTD comprises a negative differential conductance G_{rtd}, a capacitance C_{rtd}, and a series resistance R_S, which represents the Ohmic loss of contact. It is to be noted that G_{rtd} and C_{rtd} are bias dependent, while R_S is bias independent. The RTD oscillator is then formed by connecting the RTD with a resonator and an antenna. Its equivalent circuit is described in Fig. 3, where the resonator and the antenna of the oscillator are represented by the inductor L_r and antenna conductance and capacitance, G_a and C_a, respectively. The oscillation condition is satisfied if the absolute value of G_{rtd}
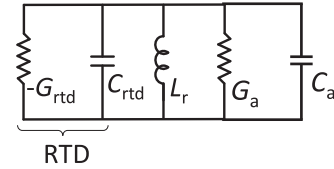

Fig. 3. Equivalent circuit of the RTD oscillator.

is equal to G_a. Under such a condition, the oscillation frequency of the oscillator is determined by the following formula:

$$f_{osc} = \frac{1}{2\pi\sqrt{L_r(C_{rtd} + C_a)}}. \tag{1}$$

Here, L_r and C_a are bias independent. The above formula indicates that, if the antenna capacitance C_a can be varied by the external feedback effect, the oscillation frequency can be changed. Moreover, G_a can also be changed by the external feedback effect leading to the change in output power, received power, and dc current of the RTD oscillator [27]. This indicates that all the parameters of the RTD oscillator, including the oscillation frequency, dc current, output power, and received power, can be varied under the effect of external feedback.

In RTD transmission systems, a hemispherical silicon (Si) lens is generally used to guide the THz beam radiated from the antenna of the RTD oscillator. In this study, the Si lens with a refractive index of 3.4 is modeled by a two-port S-parameter block, in which the magnitude and phase of S_{11} and S_{22} represent the magnitude and phase of the THz signal and the reflectivity between the Si lens surface and the air. The magnitude and phase of S_{12} and S_{21} represent the power coupling efficiency from the RTD to free space and the phase shift of the THz signal in the Si lens, respectively. These S-parameters are given as

$$\begin{pmatrix} S_{11} & S_{12} \\ S_{21} & S_{22} \end{pmatrix} = \begin{pmatrix} \Gamma_S e^{j\Phi_S} & \sqrt{\eta_S(1-\Gamma_S^2)}e^{j\Phi_{Si}} \\ \sqrt{\eta_S(1-\Gamma_S^2)}e^{j\Phi_{Si}} & \Gamma_S e^{j\Phi_S} \end{pmatrix} \tag{2}$$

where η_S denotes the power coupling efficiency from RTD to the free space, and Γ_S and Φ_S are the magnitude and phase of the THz signal reflectivity, respectively. Φ_{Si} is the phase shift in the Si lens. These S-parameters are defined to exhibit reciprocal, symmetric, passive, and lossy behaviors. They continue to hold the true in the lossless case when $\eta_S = 1$. It should be noted that the reference impedance of the S-parameters block must be equal to the characteristic impedance of the transmission line and antenna resistance $1/G_a$ for a proper circuit modeling. Here, Γ_S, η_S, Φ_S, and Φ_{Si} are introduced to take into account the effect of the multireflection and phase contribution of the system.

B. THz Link Modeling

The THz link is modeled using a transmission line, which characterizes the phase shift of the THz signal in free space, followed by an S-parameter block that characterizes the power loss due to misalignment, absorption, and polarization in the
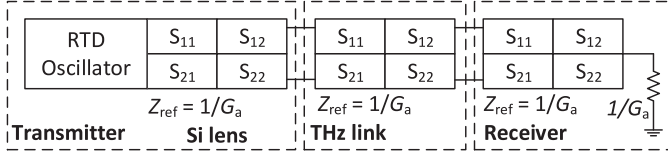
Fig. 4. Complete circuit model.

link. All the S-parameters of the THz link are given as follows:

$$\begin{pmatrix} S_{11} & S_{12} \\ S_{21} & S_{22} \end{pmatrix} = \begin{pmatrix} 0 & 1-\alpha \\ 1-\alpha & 0 \end{pmatrix} e^{j\frac{2\pi L}{\lambda_0}} \quad (3)$$

where α is the loss factor; L and λ_0 are the distance between the Tx and the Rx and the wavelength of THz wave, respectively.

C. Receiver Modeling

The Rx is also modeled with a two-port S-parameters block, in which the magnitude and phase of S_{11} and S_{22} represent the magnitude and phase of the reflectivity inside and outside the Rx antenna, respectively. The magnitude and phase of S_{12} and S_{21} represent the power coupling efficiency at the receive antenna and the phase shift inside the receive antenna, respectively. A termination, $1/G_a$, is introduced to compute the received power and render the model valid. These S-parameters are given as

$$\begin{pmatrix} S_{11} & S_{12} \\ S_{21} & S_{22} \end{pmatrix} = \begin{pmatrix} \Gamma_L e^{j\Phi_L} & \sqrt{\eta_L(1-\Gamma_L^2)}e^{j\Phi_a} \\ \sqrt{\eta_L(1-\Gamma_L^2)}e^{j\Phi_a} & 0 \end{pmatrix} \quad (4)$$

where η_L is the power coupling efficiency at the receive antenna, which is proportional to the antenna effective aperture size. Γ_L and Φ_L are the magnitude and phase of the THz signal reflectivity at the receive antenna, and Φ_a is the phase shift inside the receive antenna. Here, it is to be noted that the S-parameters of the Rx are slightly different from that of the Tx in that S_{11} represents the reflection at the receive antenna. In addition to the introduction of the load reflectivity, Γ_L and Φ_L, which are similar to that in [28], η_L and Φ_a are also included to take into account the effect of the power coupling at the Rx and the phase shift in the receive antenna. Although η_L and Φ_a have no significant impacts on the system, they are included to make the model more realistic. The reference impedance of the Rx S-parameter block is also equal to $1/G_a$.

Finally, the complete circuit model of the system, which is composed of all the above individually constructed models, is shown in Fig. 4. This model will recover to its original RTD oscillator, when there is no reflection or no external feedback in the system. In this case, the RTD will be terminated by a pure antenna impedance, $Z_A = 1/(G_a + j\omega C_a)$. In this study, the model is implemented in a popular RF circuit simulator, Keysight ADS, for efficiently performing various investigations on the effect. This is shown in detail in the following section.

D. External Feedback Modeling

In the external feedback effect, due to the superimposition of the transmitted and reflected THz signals on the RTD oscillator antenna, the capacitance and conductance of the RTD
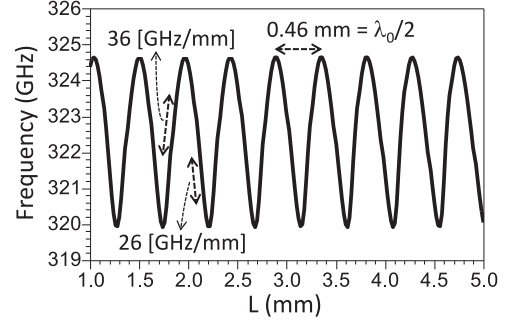

Fig. 5. Frequency change as a result of the external feedback effect. The result is derived based on the constructed model implemented in Keysight ADS.

can be changed periodically. A change in the antenna capacitance causes a change in the oscillation frequency, whereas a change in the antenna conductance causes a change in the received power and dc current of the RTD oscillator. Among these changes, the frequency and received power changes are the dominant parameters for applications such as sensing and wireless communication. The change in the dc current is useful for other applications such radar or sensing. In this section, the dominant factors of the system, which cause frequency, received power, and dc current changes, are clarified based on the above-constructed model. For this, important criteria, such as the magnitude and rate of the change, should be defined initially. Here, it should be noted that we only investigated frequency characteristic in [28] due to the simplicity of the RTD model. This simple RTD with a polynomial current model and a constant capacitance model could not accurately explain the power and dc current changes. In the present study, by using a more complex RTD model, not only frequency but also power and dc current have been investigated carefully. Fig. 5 illustrates the simulated results for the frequency change under the external feedback effect. Here, the reflectivity at the Rx and the Tx is set to 9% and 25%, respectively. It can be observed that, when the distance between the Tx and the Rx varies from 1 to 5 mm, the frequency changes periodically with a period of half wavelength, 0.46 mm. The magnitude of the change is 2.5 GHz. There are two asymmetrical rates of change: 36 and 26 GHz/mm. These rates are defined as the derivatives of the frequency with respect to the distance. This indicates that, if the distance between the Tx and the Rx varies by only 0.05 mm or 5.4% of λ, where $\lambda = 0.93$ mm is oscillation wavelength, the frequency can be changed remarkably by 1.8 and 1.3 GHz, respectively. The change and change rate will cause serious issues for wireless communication systems using frequency- or phase-based modulation schemes, such as QAM and QPSK. On the other hand, they can be utilized to sense the parameters of the system such as the reflectivities at the Tx and the Rx. This is highly beneficial because, in practice, the system parameters are difficult to measure. Here, it is to be noted that the present model is basically different from the analysis in [28], where the frequency change is governed by a sinusoidal form; however, in the present model, it can be not only sinusoidal, but also asymmetrical, depending on the strength of the external feedback. This asymmetrical form arises from the different contributions of the reflectivities at the Tx and the Rx of
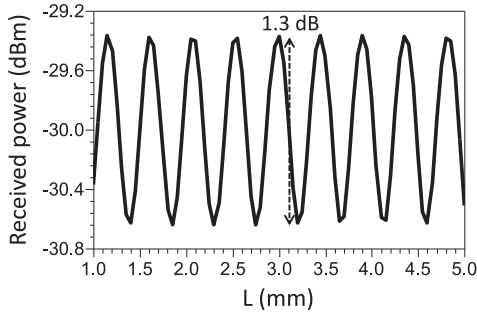
Fig. 6. Received power change as a result of the external feedback effect. The result is derived based on the constructed model implemented in Keysight ADS.
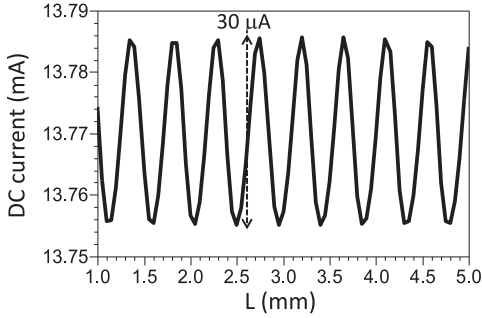

Fig. 7. DC current change as a result of the external feedback effect. The result is derived based on the constructed model implemented in Keysight ADS.
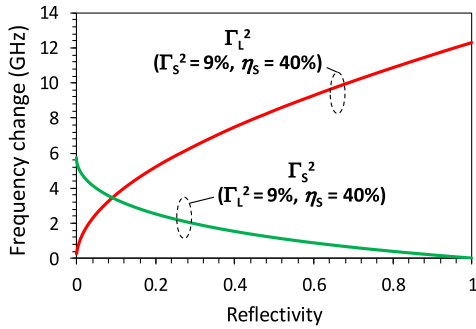

Fig. 8. Frequency change as a function of the reflectivities at the Rx (Γ_L) and the Tx (Γ_S).

Fig. 9. Frequency change as a function of the power coupling efficiencies at the Tx (η_S) and the Rx (η_L).

Fig. 10. Frequency change rate as a function of the reflectivities at the Rx (Γ_L) and the Tx (Γ_S).

Fig. 11. Frequency change rate as a function of the power coupling efficiencies at the Tx (η_S) and the Rx (η_L).

the system or the multireflection, which is ignored in [28]. In addition to the frequency change, Figs. 6 and 7 describe how the external feedback causes changes in the received power and dc current, respectively. Here, the power and current changes are 1.3 dB and 30 μA, respectively. Although these changes are relatively small, they are sufficient to affect the system performance.

1) Frequency Change: Among the system factors, the frequency change should be mainly dependent on the magnitude of the reflectivity at both the Tx (Γ_S) and the Rx (Γ_L) and the power coupling efficiency at the RTD (η_S) because these factors contribute to the external feedback strength of the system. This is demonstrated in Figs. 8 and 9, which illustrate the change in frequency with the reflectivities Γ_L, Γ_S, and the power coupling efficiencies at the Tx (η_S) and the Rx (η_L), respectively. These figures show that the change with Γ_L is largest compared to those with Γ_S, η_S, and η_L. This indicates that Γ_L is the dominant
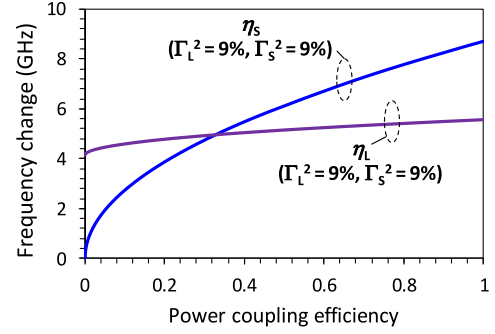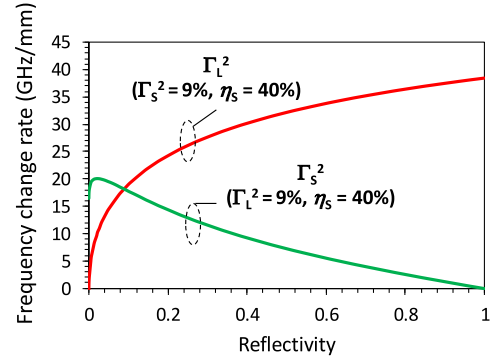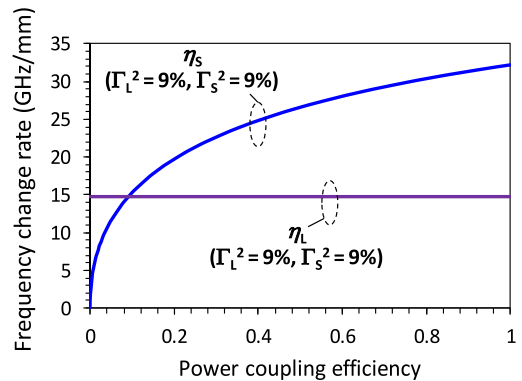
factor for the frequency change. Furthermore, the frequency change increases on increasing R_L and η_S but on decreasing Γ_S. This is because increasing Γ_L and η_S, and decreasing Γ_S causes the power reflected back to the RTD to increase, resulting in strong feedback. Another important point here is that the change becomes zero if $\Gamma_L = \eta_S = 0$ and $\Gamma_S^2 = 1$. This is because, if there is no reflection at the Rx, no power coupled to free space, or no power reflected back to the RTD, the oscillation frequency becomes stable.

2) Frequency Change Rate: Similar to the frequency change, the frequency change rate mainly depends on Γ_L, Γ_S, and η_S. Figs. 10 and 11 show the impact of the reflectivity (Γ_L, Γ_S) and power coupling efficiency (η_L, η_S) on the frequency
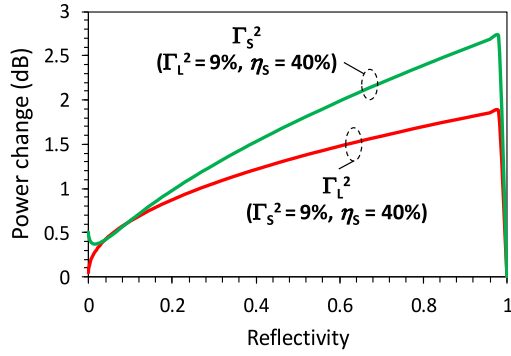
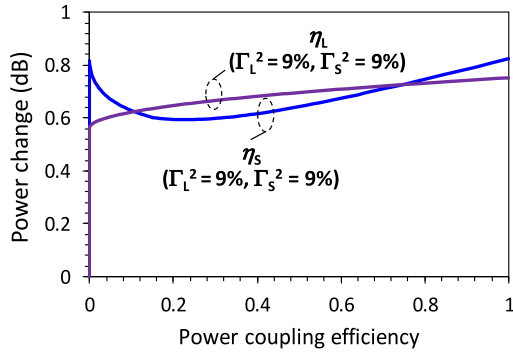Fig. 12. Received power change as a function of the reflectivities at the Rx (Γ_L) and the Tx (Γ_S).

Fig. 13. Received power change as a function of the power coupling efficiencies at the Rx (η_L) and the Tx (η_S).

Fig. 14. DC current change as a function of the reflectivities at the Rx (Γ_L) and the Tx (Γ_S).

Fig. 15. DC current change as a function of the power coupling efficiencies at the Rx (η_L) and the Tx (η_S).

Fig. 16. Simulated oscillation frequency of the RTD and ideal systems.

change rate, respectively. These figures indicate that Γ_L once again is the dominant factor and η_S is the second dominant factor. Furthermore, the behavior of these parameters is similar to that of the frequency change.

In summary, it can be concluded that the frequency change and frequency change rate are mainly affected by the reflectivity at the Rx, whereas the power coupling efficiency is the second dominant factor contributing to these changes.

3) Received Power Change: In this section, the change in the received power is investigated. It is to be noted that for the received power, the change is more important than the rate. The received power change with the distance is illustrated in Figs. 12 and 13. The figures indicate that the reflectivity at the Tx (Γ_S) is the dominant factor, whereas the power coupling efficiency at the Tx and the Rx (η_L and η_S) has no significant contribution to the received power change. It can be seen that, when the reflectivity at the Tx and the Rx reaches 100%, the received power change becomes zero because, when $\Gamma_L = 1$, there is no power received by the load, whereas, when $\Gamma_S = 1$, there is no power radiated to the free space. In addition, when $\Gamma_L = 0$ and $\eta_L = 0$, $\eta_S = 0$, the received power change also becomes zero. This can be explained as follows: when $\Gamma_L = 0$, there is no feedback effect; when $\eta_L = 0$, there is no power entering the Rx; and when $\eta_S = 0$, there is no signal coupled to free space.

4) DC Current Change: Besides the change in frequency and power, external feedback also causes the dc current in the RTD to change due to the change in antenna conductance. The change in the dc current under the effect of the reflectivity
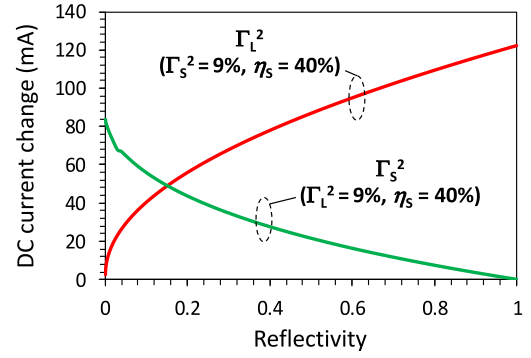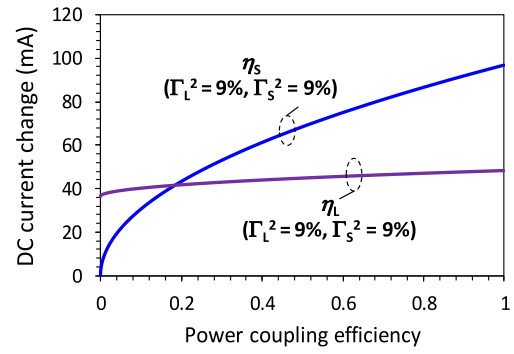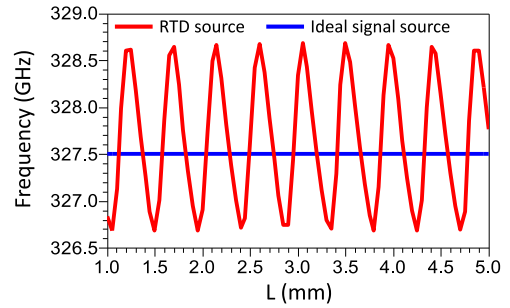
(Γ_L, Γ_S) and power coupling efficiency (η_L, η_S) is shown in Figs. 14 and 15. It can be seen that all the behaviors of the dc current change are similar to that of the frequency change magnitude. Here, once again, the dominant factor is the reflectivity at the Rx (Γ_L).

From the above discussions, it is obvious that the external feedback affects not only the frequency, but also the received power and dc current of the RTD oscillator. However, in a conventional system [29], where an ideal signal source is used, external feedback can still occur. In such a system, although the frequency and dc current do not change with the distance, the received power can still change due to the external feedback between the Tx and the Rx. This is demonstrated in Figs. 16 and 17, which show the comparison of the external feedback between an RTD and an ideal system. Here, it is to be noted that the ideal and RTD systems are identical, except that the ideal
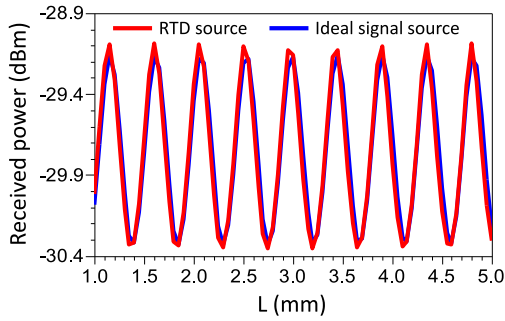
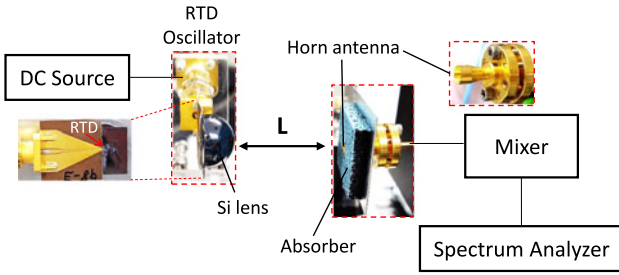Fig. 17.   Simulated received power of the RTD and ideal systems.

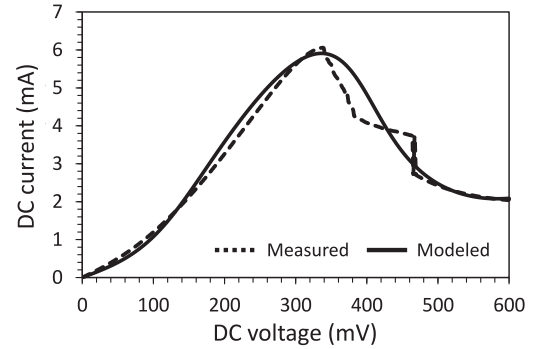Fig. 18.   Experimental setup.

Fig. 19.   Measured and simulated current–voltage characteristics of the RTD.

Fig. 20.   Measured and simulated oscillation frequency of the RTD oscillator.

system uses an ideal signal source instead of using the RTD source as in the RTD system. The ideal signal source is different from that of the RTD source in that its frequency and bias condition are stable. In the RTD system, it can be observed that both the frequency and received power can change, whereas in the ideal system, only the received power changes and its frequency remains unchanged. This finding is crucial for short-distance wireless communication because in such applications, the bit error rate (BER), which is defined as the number of bit errors per unit time, can be easily changed due to external feedback. Using the proposed model, the origins of this phenomenon, not only for the RTD system but also for conventional systems, can be clarified.

III. EXPERIMENTAL VALIDATION

A. Experimental Setup

To validate the accuracy of the constructed model, the experiment depicted in Fig. 18 is set up to measure the changes in the oscillation frequency, the dc current, and the received power of an RTD oscillator. An unmodulated THz signal radiated from the dipole antenna of the RTD oscillator through an Si lens was received by a circular horn antenna, which is connected to a commercial mixer system through a WR-2.8 rectangular metallic hollow waveguide. The received signal was then down-converted to an intermediate frequency by a commercial mixer for display on a spectrum analyzer (SA), where the oscillation frequency and received power were measured. The dc current was measured on a dc power supply. Here, an RTD of 1.6 μm^2 in size was connected to a dipole antenna to form a THz oscillator. Detailed descriptions of this device are given in [30]. To realize precise measurements and reliable data aggregation, the step size of the spacing between the RTD oscillator and the Rx must be considerably smaller than the standing wave period
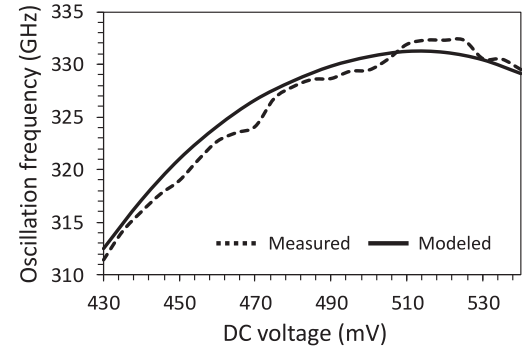
($\lambda_0/2$), with λ_0 being the THz wavelength. In the measurement, the step size is set to 0.05 mm, which is approximately $\lambda_0/18$. This is sufficient to achieve precise and reliable data aggregation. In addition, when the THz beam reaches the horn antenna of the mixer system, complex reflection can occur at the horn antenna edge and flange owing to their complex metallic structure [32]. Hence, an absorber was used to suppress this complex reflection, resulting in clean measured data.

B. DC and RF Characteristics

The measured dynamic and modeled static current–voltage characteristics of the RTD are shown in Fig. 19, and its measured and modeled oscillation frequency are depicted in Fig. 20. In the negative differential resistance (NDR) region, the measured current–voltage deviates from the simulated one because in this region, the RTD oscillates, rendering it impossible to measure the static values [31]. Excellent agreement between the model and measurement is clearly observed, validating the model in terms of both the dc and RF characteristics. It is worth noting that while the simple RTD model in [28] has a constant capacitance model, the present study employs a complex RTD model with a voltage-dependent capacitance model. This causes both the dc and RF characteristics to be fitted well with measurements in the entire bias range, as shown in Figs. 19 and 20.

C. External Feedback Effect

After the dc and RF validation, the model is validated for the external feedback in this section. In the present study, frequency, power, and dc current changes by the external feedback were
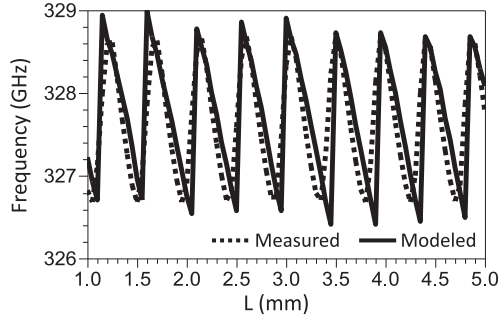
Fig. 21. Measured and simulated results of the change in the frequency with the distance.
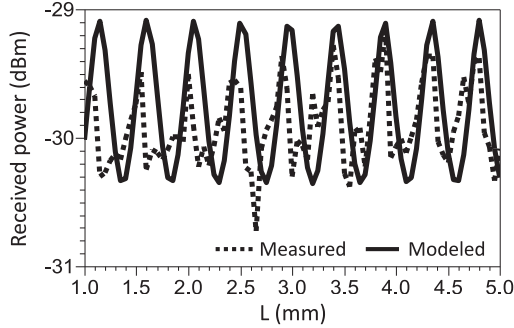

Fig. 22. Measured and simulated results of the change in the received power with the distance.
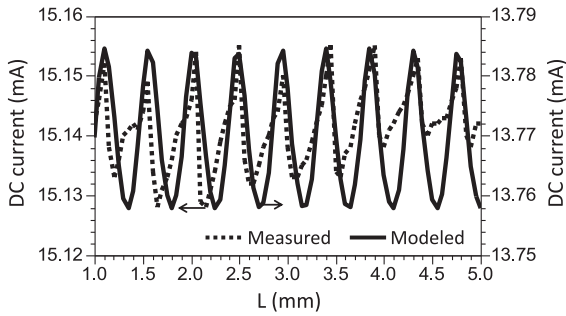

Fig. 23. Measured and simulated results of the change in the dc current with the distance.

experimentally validated. This contrasts to the result presented in [28], where only frequency characteristic was validated with measurement. The following realistic parameters should be used in the model: the power reflectivity outside the Si lens surface is $\Gamma_S^2 = 30\%$ owing to the reflection at the boundary of two materials having different refractive indices (3.4 of Si and 1 of air); the phase of the reflectivity outside the Si lens surface should be π owing to the phase change at the reflective boundary. The other parameters, including the reflectivity at the horn antenna, the power coupling efficiency at the oscillator and horn antenna, the power loss due to misalignment, absorption, and polarization, and the phase shift in the Si lens, are the fitting parameters. The validation for external feedback is shown in Figs. 21–23. Here, the fitting parameters are $\Phi_{Si} = 1.45\pi$, $\Gamma_L^2 = 7\%$, $\eta_S = 42\%$, and $\alpha = 30\%$. Good agreement between the modeled and measured data can be observed in these figures.
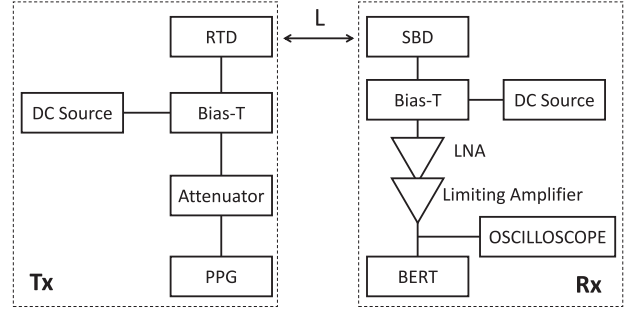

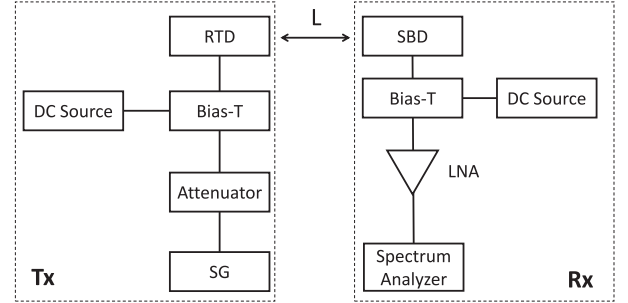
Fig. 24. Experimental setup for BER measurement.

Fig. 25. Experimental setup for detected power measurement.

Although the changes in the power and dc current are relatively small, the model can still well describe these changes. There is some deviation between the simulated and measured results because of the imperfection in dc and RF fitting parameters of the RTD model. Here, it is to be noted that the changes in the power and dc current are measured simultaneously with the change in frequency. This demonstrates that the model succeeds in describing the feedback effect of the system. In the following section, the causes for the change in the BER of a wireless communication system are specified, based on the constructed model. As discussed in Section II-D, in proximity wireless communication, one of the important issues is the periodical change of the BER with the distance between the Tx and the Rx due to the external feedback effect. This change will degrade the quality of communication. Therefore, determining the origins of this change becomes critical.

IV. APPLICATION DEMONSTRATION

A. Wireless Communications

Figs. 24 and 25 show the experimental setups for measurement of BER and received power, respectively. In the BER measurement setup, the Tx was the RTD, while the Rx used a commercial Virginia Diodes, Inc. Schottky barrier diode (SBD). The BER is measured using a BER Tester (BERT), an instrument used for testing the BER, after the baseband signal was passed through a low-noise amplifier (LNA) with a power gain of 50 dB and a limiting amplifier for shaping the signal. In the detected power measurement setup, the RTD Tx was used but without the pulse pattern generator (PPG), while in the Rx side, an SBD was used to detect the received power from the Tx, and the detected power was then displayed on a SA. Fig. 26
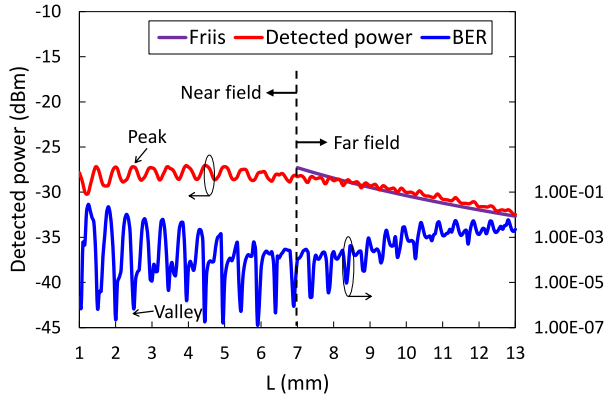
Fig. 26.   Measured results of BER and detected power.

Fig. 27.   Calculated and measured BER.

Fig. 28.   Calculated and measured detected power.

shows the measured results for the BER and detected power of the system. In the BER measurement, the baseband signal had a data rate of 1 Gb/s, with the power of 7 dBm. The RTD was biased in the NDR region with a bias voltage of -519.5 mV. In the detected power measurement, a sinusoidal signal with frequency of 1 GHz was directly modulated in the RTD. Here, the RTD was again biased in the NDR region. From the figure, it can be clearly seen that the received power and BER periodically change with the distance between the Tx and the Rx due to the external feedback. Moreover, a theoretical received power curve using the Friis transmission equation is also shown in the figure to determine the near field and far field of the communications. When calculating the received power using the Friis transmission equation [33], the gain of the transmit system was 20 dBi, whereas that of the receive antenna was 23 dBi. These values were evaluated by electromagnetic field simulation. As can be seen in the figure, the near-field communication, in this case, is determined within a distance of 7 mm.

In this region, when the received power is maximal, the BER becomes minimal. In addition, the BER decreases with the increase in detected power. The far-field communication is defined by fitting the detected power curve with the Friis transmission equation. From these discussions, it can be concluded that the received power should be the dominant factor that causes BER fluctuation. To demonstrate the validity of this conclusion, the detected power and BER are calculated using the following formula [32], [34]:

$$P_{\mathrm{d}} = \frac{P_{\max}}{1 + \frac{4 R_{\mathrm{eff}}}{(1 - R_{\mathrm{eff}})^2} \sin^2\left(\frac{2\pi L}{\lambda}\right)} \tag{5}$$

$$\mathrm{BER}\left(R_{\mathrm{eff}}, L\right) = \mathrm{BER}_0 \exp\left[\left\{\ln\left(\frac{1}{2}\right) - \ln(\mathrm{BER}_0)\right\}\right.$$
$$\left. \times \left\{1 - \frac{1}{F\left(R_{\mathrm{eff}}, L\right)}\right\}\right] \tag{6}$$

where

$$F\left(R_{\mathrm{eff}}, L\right) = 1 + \frac{4 R_{\mathrm{eff}}}{(1 - R_{\mathrm{eff}})^2} \sin^2\left(\frac{2\pi L}{\lambda}\right). \tag{7}$$

P_{d} is calculated based on the Fabry–Pérot's etalon theory, whereas the BER is calculated with the assumption that the
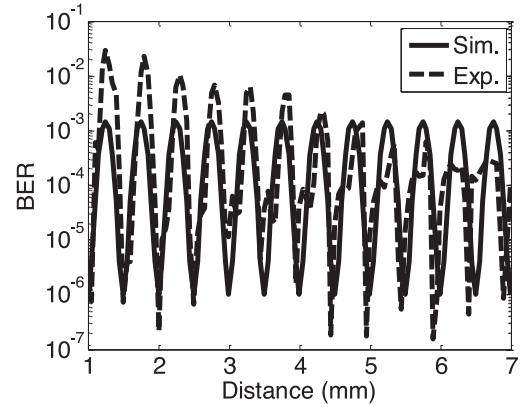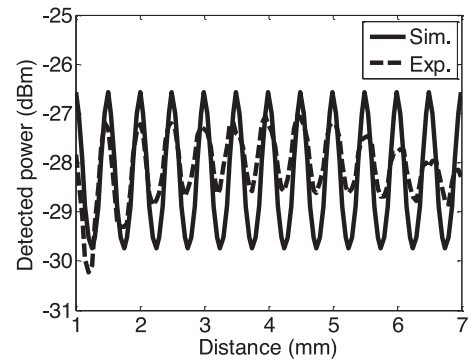
simple ON–OFF keying modulation scheme is used in the present system. In these formulas, $P_{\max}$ and λ are the maximum detected power and wavelength, respectively. L is the mirror spacing and R_{eff} is the effective reflectivity. The calculated results in Figs. 27 and 28 are obtained using the following parameters: $\mathrm{BER}_0 = 10^{-6}$, $R_{\mathrm{eff}} = 0.2$, $\lambda = 1$ mm, and $P_{\max} = -26$ dBm. The calculated and measured results for BER and detected power are shown in Figs. 27 and 28, respectively. Both the calculations and measurements indicate that the changes in the BER and received power are out of phase. Moreover, the calculated magnitude of the detected power and the BER is consistent with the measured ones in the near field. It is important to note that there is certain deviation between the simulated and calculated detected power, and this is attributed to the misalignment between the RTD Tx and the SBD Rx. Nevertheless, the above discussions verify the conclusion in Section II-D that the detected power is the dominant factor in BER fluctuation. This finding can assist in proposing solutions for suppressing the external feedback by considering receive antenna design for low reflection.

V. Conclusion

In this paper, a complete system model is developed for describing the external feedback effect in an RTD oscillator. The modeled results agree well with the experimental ones not only for the change in the oscillation frequency, but also for those in the received power and dc current. The frequency change, the

frequency change rate, and the dc current change are mainly affected by the reflectivity at the Rx. The change in the received power is mainly due to the reflectivity at the Tx. The model is used to demonstrate a possible application in THz proximity wireless communication. Using the model, the origin of the BER change with the distance is determined to be due to the received power change. Thus, a stable THz wireless communication system can be designed using the proposed model. Moreover, by sensing system properties such as the reflectivities at the Tx and the Rx, the model can be used in THz sensing applications. Finally, the ability to model the change in the dc current of the system can be utilized for THz short-range radar applications.

REFERENCES

[1] M. Tonouchi, "Cutting-edge terahertz technology," *Nature Photon.*, vol. 1, pp. 77–105, Feb. 2007.

[2] T. Nagatsuma, "Terahertz technologies: Present and future," *IEICE Electron. Express*, vol. 8, no. 14, pp. 1127–1142, Jul. 2011.

[3] K. B. Cooper *et al.*, "THz imaging radar for standoff personnel screening," *IEEE Trans. THz Sci. Technol.*, vol. 1, no. 1, pp. 169–182, Sep. 2011.

[4] K. Ajito and Y. Ueno, "THz chemical imaging for biological applications," *IEEE Trans. THz Sci. Technol.*, vol. 1, no. 1, pp. 293–300, Sep. 2011.

[5] I. Kallfass *et al.*, "All active MMIC-based wireless communication at 220 GHz," *IEEE Trans. THz Sci. Technol.*, vol. 1, no. 2, pp. 477–487, Nov. 2011.

[6] T. Nagatsuma *et al.*, "Terahertz wireless communications based on photonics technologies," *Opt. Express*, vol. 21, no. 20, pp. 23736–23747, Sep. 2013.

[7] Z. D. Taylor *et al.*, "THz and mm-Wave sensing of corneal tissue water content: In vivo sensing and imaging results," *IEEE Trans. THz Sci. Technol.*, vol. 5, no. 2, pp. 184–196, Feb. 2015.

[8] T. Nagatsuma *et al.*, "Millimeter-wave and terahertz-wave applications enabled by photonics," *IEEE J. Quantum Electron.*, vol. 52, no. 1, pp. 1127–1142, Jan. 2016.

[9] J. Treuttel *et al.*, "A 520-620-GHz Schottky receiver front-end for planetary science and remote sensing with 1070 K-1500 K DSB noise temperature at room temperature," *IEEE Trans. THz Sci. Technol.*, vol. 6, no. 1, pp. 148–155, Jan. 2016.

[10] T. Nagatsuma, G. Ducournau, and C. C. Renaud, "Advances in terahertz communications accelerated by photonics," *Nature Photon.*, vol. 10, no. 6, pp. 371–379, May 2016.

[11] S. Rosenbaum *et al.*, "155-and 213-GHz AlInAs/GaInAs/InP HEMT MMIC oscillators," *IEEE Trans. Microw. Theory Techn.*, vol. 43, no. 4, pp. 927–932, Apr. 1995.

[12] V. Radisic *et al.*, "Demonstration of sub-millimeter-wave fundamental oscillators using 35-nm InP HEMT technology," *IEEE Microw. Wireless Compon. Lett.*, vol. 17, no. 3, pp. 223–225, Mar. 2007.

[13] Benjamin S. Williams, "Terahertz quantum-cascade lasers," *Nature Photon.*, vol. 1, pp. 517–525, Sep. 2007.

[14] M. Asada, S. Suzuki, and N. Kishimoto, "Resonant tunneling diodes for sub-terahertz and terahertz oscillators," *Jpn. J. Appl. Phys.*, vol. 47, no. 6, pp. 4375–4384, Jun. 2008.

[15] K. Okada, K. Kasagi, N. Oshima, S. Suzuki, and M. Asada, "Resonant-tunneling-diode terahertz oscillator using patch antenna integrated on slot resonator for power radiation," *IEEE Trans. THz Sci. Technol.*, vol. 5, no. 4, pp. 613–618, Jul. 2011.

[16] M. Seo *et al.*, "InP HBT IC technology for terahertz frequencies: Fundamental oscillators up to 0.57 THz," *IEEE J. Solid-State Circuits*, vol. 46, no. 10, pp. 2203–2214, Oct. 2011.

[17] T. Maekawa, H. Kanaya, S. Suzuki, and M. Asada, "Oscillation up to 1.92 THz in resonant tunneling diode by reduced conduction loss," *Appl. Phys. Express*, vol. 9, no. 2, pp. 1–4, Jan. 2016.

[18] T. Mukai, M. Kawamura, T. Takada, and T. Nagatsuma, "1.5-Gbps wireless transmission using resonant tunneling diodes at 300 GHz," in *Proc. Int. Conf. Opt. Terahertz Sci. Technol.*, Mar. 2011, Paper MF42.

[19] K. Ishigaki *et al.*, "Direct intensity modulation and wireless data transmission characteristics of terahertz-oscillating resonant tunnelling diodes," *Electron. Lett.*, vol. 48, no. 10, pp. 582–583, May 2012.

[20] T. Nagatsuma, M. Fujita, A. Kaku, D. Tsuji, and S. Nakai, "Terahertz wireless communication using resonant tunneling diodes as transmitters and receivers," in *Proc. 3rd Int. Conf. Telecommun. Remote Sens.*, Jun. 2014, pp. 41–46.

[21] N. Oshima, K. Hashimoto, S. Suzuki, and M. Asada, "Wireless data transmission of 34 Gbit/s at a 500-GHz range using resonant-tunnelling-diode terahertz oscillator," *Electron. Lett.*, vol. 52, no. 22, pp. 1897–1898, Oct. 2016.

[22] S. Diebold *et al.*, "High-speed error-free wireless data transmission using a terahertz resonant tunneling diode transmitter and receiver," *Electron. Lett.*, vol. 52, no. 24, pp. 1999–2001, Nov. 2016.

[23] K. Okada, K. Kasagi, N. Oshima, S. Suzuki, and M. Asada, "Terahertz wireless data transmission with frequency and polarization division multiplexing using resonant-tunneling-diode oscillators," *IEEE Trans. THz Sci. Technol.*, vol. 7, no. 5, pp. 593–598, Sep. 2017.

[24] T. Miyamoto, A. Yamaguchi, and T. Mukai, "Terahertz imaging system with resonant tunneling diodes," *Jpn. J. Appl. Phys.*, vol. 55, Jan. 2016, Art. no. 032201.

[25] K. Okamoto *et al.*, "Terahertz sensor using photonic crystal cavity and resonant tunneling diodes," *J. Infrared, Millimeter, Terahertz Waves*, vol. 38, no. 9, pp. 1085–1097, Sep. 2017.

[26] T. Schneider, A. Wiatrek, S. Preuler, M. Grigat, and R. P. Braun, "Link budget analysis for terahertz fixed wireless links," *IEEE Trans. THz Sci. Technol.*, vol. 2, no. 2, pp. 250–256, Aug. 2012.

[27] M. Asada and S. Suzuki, "Theoretical analysis of external feedback effect on oscillation characteristics of resonant-tunneling-diode terahertz oscillators," *Jpn. J. Appl. Phys.*, vol. 54, Jun. 2015, Art. no. 070309.

[28] L. D. Manh *et al.*, "Modeling of external feedback effect of resonant tunneling diode oscillator for terahertz applications," *IEICE Tech. Rep.*, vol. 116, no. 297, pp. 7–12, Nov. 2016.

[29] T. Nagatsuma, K. Oogimoto, Y. Inubushi, and J. Hirokawa, "Practical considerations of terahertz communications for short distance applications," *Nano Commun. Netw.*, vol. 10, pp. 1–12, Sep. 2016.

[30] S. Diebold *et al.*, "Modeling and simulation of terahertz resonant tunneling diode-based circuits," *IEEE Trans. THz Sci. Technol.*, vol. 6, no. 5, pp. 716–723, Aug. 2016.

[31] S. Diebold, M. Fujita, and T. Nagatsuma, "Asymmetrical conductance model to analyze resonant tunneling diode terahertz oscillators," *IEEE Trans. THz Sci. Technol.*, vol. 6, no. 5, pp. 716–723, Aug. 2016.

[32] R. Kakimi, M. Fujita, M. Nagai, M. Ashida, and T. Nagatsuma, "Capture of a terahertz wave in a photonic-crystal slab," *Nature Photon.*, vol. 8, pp. 657–663, Jul. 2014.

[33] S. J. Orfanidis, "Free space propagation," in *Millimetre Wave Antennas for Gigabit Wireless Communications: A Practical Guide to Design and Analysis in a System Context*, 1st ed. Hoboken, NJ, USA: Wiley, 2008, ch. 1, sec. 1.3.1, pp. 12–14.

[34] H. Takahashi, T. Kosugi, A. Hirata, K. Murata, and N. Kukutsu, "10-Gbit/s BPSK modulator and demodulator for a 120-GHz-band wireless link," *IEEE Trans. Microw. Theory Techn.*, vol. 59, no. 5, pp. 1361–1368, Jan. 2011.

Luong Duy Manh (M'13) received the B.S. and M.S. degrees in physics from the Hanoi University of Science (a member of Vietnam National University), Hanoi, Vietnam, in 2005 and 2007, respectively, and the D.E. degree in electronics engineering from the University of Electro-Communications, Tokyo, Japan, in March 2016.

He was a Postdoctoral Researcher with the Graduate School of Engineering Science, Osaka University, Osaka, Japan, from April 2016 to June 2017. He is currently a Lecturer with Le Quy Don Technical University, Hanoi. His research interests include the development of microwave semiconductor devices and circuits and terahertz integrated systems for wireless communication applications based on resonant tunneling diodes and photonic crystals.

Sebastian Diebold (GS'11–M'13) received the Dipl.-Ing, and Dr.-Ing. degrees in electrical engineering and information technology from the Karlsruhe Institute of Technology (KIT), Karlsruhe, Germany, in 2009 and 2013, respectively.

In 2009, he was with the Fraunhofer Institute for Applied Solid-State Physics (IAF), Freiburg, Germany. From 2010 to 2014, he was a Research Associate and Teaching Assistant with KIT. He was involved in characterization and modeling of passive and active components and in the development of millimeter-wave monolithic integrated circuits and systems at both Fraunhofer IAF and KIT. In 2014, he joined the Graduate School of Engineering Science, Osaka University, Osaka, Japan, as a Research Fellow of the Japan Society for the Promotion of Science. In 2016, he became an Assistant Professor with Osaka University, where he was involved with terahertz (THz) oscillating devices using resonant tunneling diodes and integrated THz-wave systems and antenna designs. In 2017, he joined pSemi (a Murata Company), San Diego, CA, USA, as a Millimeter-Wave Monolithic Integrated Circuit Design Engineer.

Kousuke Nishio received the B.E. and M.E. degrees in engineering science from Osaka University, Osaka, Japan, in 2015 and 2017, respectively.

He was involved in research on integrated terahertz wireless communication systems using resonant tunneling diodes.

Yousuke Nishida received the B.E. and M.E. degrees in engineering science from Osaka University, Osaka, Japan, in 2016 and 2018, respectively.

He was involved in research on integrated terahertz wireless communication systems using resonant tunneling diodes.

Jaeyoung Kim received the B.S., M.S., and Ph.D. degrees in electrical and electronic engineering from Yonsei University, Seoul, South Korea, in 2004, 2006, and 2011, respectively.

For his Ph.D. dissertation, he investigated integrated circuits and optoelectronics for millimeter-wave wireless communication. In 2011, he began his career with NTT Microsystem Integration Laboratories, NTT Corporation, Atsugi, Japan, where he studied InP monolithic microwave integrated circuits for 300-GHz-band wireless transceiver and terahertz (THz) frequency-domain spectroscopy and imaging systems. In 2014, he joined the Research and Development Division, ROHM Co., Ltd., Kyoto, Japan, to work on solid-state THz transceivers using resonant tunneling diodes for sensor and communication applications. His research interests include millimeter-wave and THz systems for wireless communication, sensing, and imaging applications based on photonic and high-speed electronic technologies.

Toshikazu Mukai received the M.E. degree in engineering science from Osaka University, Osaka, Japan, in 2005.

In 2005, he joined ROHM Co., Ltd., Kyoto, Japan. He was involved in developing SiC power devices for three years. He has studied the engineering of resonant tunneling diodes as terahertz oscillators and detectors for terahertz applications.

Masayuki Fujita (S'00–M'02) received the B.E., M.E., and Ph.D. degrees in electrical and computer engineering from Yokohama National University, Yokohama, Japan, in 1997, 1999, and 2002, respectively.

During his Ph.D. research, he achieved the first room-temperature continuous-wave operation of microdisk lasers and the lowest threshold current of 40 μA in GaInAsP lasers. He also proposed and demonstrated a microgear laser. In 2002, he joined the Quantum Optoelectronics Laboratory, Kyoto University, as a Postdoctoral Fellow and started research on photonic crystals, including spontaneous emission control in a photonic crystal and highly efficient light extraction in light-emitting diodes and silicon light emitters. From 2006 to 2010, he was an Assistant Professor, and from 2010 to 2011, a Senior Lecturer with the Department of Electronic Science and Engineering, Kyoto University. He is currently an Associate Professor with the Division of Advanced Electronics and Optical Science, Department of Systems Innovation, Graduate School of Engineering Science, Osaka University, Osaka, Japan. His research interests include terahertz photonic materials and devices and photonic nanostructures and microstructures.

Prof. Fujita is a member of the Japan Society of Applied Physics (JSAP), the Laser Society of Japan, the Institute of Electronics, Information and Communication Engineers, Japan, and the Japanese Photochemistry Association. From 1999 to 2002 and from 2003 to 2006, he was a Research Fellow with the Japan Society for the Promotion of Science. In 2015, he became the Research Director of the strategic basic research programs (Core Research for Evolutional Science and Technology) of the Japan Science and Technology Agency. He was the recipient of various awards, including the Best Student Paper Award from the Optoelectronic and Communication Conference in 2000, the JSAP Scientist Presentation Award in 2001, the JSAP Young Scientist Award in 2006, a Research Award from the Research Foundation for Opto-Science and Technology in 2007, a Paper Award from the Laser Society of Japan in 2007, and the Osaka University Presidential Awards for Encouragement in 2013–2015.

Tadao Nagatsuma (M'93–SM'02–F'15) received the B.S., M.S., and Ph.D. degrees in electronic engineering from Kyushu University, Fukuoka, Japan, in 1981, 1983, and 1986, respectively.

In 1986, he joined the Electrical Communications Laboratories, Nippon Telegraph and Telephone Corporation (NTT), Atsugi, Japan. From 1999 to 2002, he was a Distinguished Technical Member with NTT Telecommunications Energy Laboratories. From 2003 to 2007, he was a Group Leader with NTT Microsystem Integration Laboratories, and was an NTT Research Professor from 2007 to 2009. Since 2007, he has been with Osaka University, Osaka, Japan, where he is currently a Professor with the Division of Advanced Electronics and Optical Science, Department of Systems Innovation, Graduate School of Engineering Science and a Director of the Co-Creative Education Division, Office for Industry-University Co-Creation. His research interests include ultrafast electronics and millimeter-wave and terahertz photonics.

Dr. Nagatsuma is a Fellow of the Institute of Electronics, Information and Communication Engineers (IEICE), Japan, and the Electromagnetics Academy. He is an Associate Editor for IEEE PHOTONICS TECHNOLOGY LETTERS and an IEEE MTT-S Distinguished Microwave Lecturer. He was the Director of the IEICE from 2015 to 2017. He is a member of the IEEE Microwave Photonics Conference Steering Committee and the IEEE Microwave Theory and Technique Technical Committees, MTT-3: Microwave Photonics, and MTT-4: Terahertz Technology and Applications. He was the recipient of numerous awards including the 1989 IEICE Young Engineers Award, the 1992 IEEE Andrew R. Chi Best Paper Award, the 1997 Okochi Memorial Award, the 1998 Japan Microwave Prize, the 2000 Ministers Award of the Science and Technology Agency, the 2002 and 2011 Asia–Pacific Microwave Conference Prize, the 2004 Yokosuka Research Park Award, the 2006 Asia–Pacific Microwave Photonics Conference Award, the 2006 European Microwave Conference Prize, the 2007 Achievement Award presented by the IEICE, the 2008 Maejima Award, the 2011 Recognition from Kinki Bureau of Telecommunications, Ministry of Internal Affairs and Communications, the 2011 Commendation for Science and Technology by the Ministry of Education, Culture, Sports, Science and Technology, and the 2014 IEEE Tatsuo Ito Award.